Materials Science and Engineering C 63 (2016) 671–677

Contents lists available at ScienceDirect

Materials Science and Engineering C

journal homepage: www.elsevier.com/locate/msec

A new titanium based alloy Ti–27Nb–13Zr produced by powder metallurgy with biomimetic coating for use as a biomaterial

Marcio W.D. Mendes *, Carola G. Ágreda, Ana H.A. Bressiani, José C. Bressiani

Materials Science and Technology Center, Energy and Nuclear Research Institute, Av. Lineu Prestes 2242, C.P: 05508-000 São Paulo, SP, Brazil

ARTICLE INFO

Article history:
Received 16 December 2015
Received in revised form 14 February 2016
Accepted 15 March 2016
Available online 17 March 2016

Keywords:
Titanium alloy
Ti–Nb–Zr
powder metallurgy
Young's modulus
Apatite coating

ABSTRACT

Titanium alloys are widely used in biomedical applications due to their excellent properties such as high strength, good corrosion resistance and biocompatibility. Titanium alloys with alloying elements such as Nb and Zr are biocompatible and have Young's modulus close to that of human bone. To increase the bioactivity of titanium alloy surfaces is used chemical treatment with NaOH followed by immersion in simulated body fluid (SBF). The purpose of this study was to produce the alloy Ti–27Nb–13Zr with low Young's modulus by powder metallurgy using powders produced by the HDH process. The formation of biomimetic coatings on samples immersed in SBF for 3, 7, 11 and 15 days was evaluated. Characterization of the coating was performed by diffuse reflectance infrared Fourier transform spectroscopy (DRIFTS) and scanning electron microscope. The microstructure and composition of the alloy were determined using SEM and XRD, while the mechanical properties were evaluated by determining the elastic modulus and the Vickers microhardness. The sintered alloys were composed of α and β phases, equiaxed grains and with density around 97.8% of its theoretical density. The Vickers microhardness and elasticity modulus of the alloy were determined and their values indicate that this alloy can be used as a biomaterial. Analysis of the coating revealed the presence of calcium phosphate layers on samples immersed for >3 days in the SBF solution.

1. Introduction

Titanium alloys for implants with good biocompatibility, longer lifetime in the human body environment, Young's modulus compatible with that of human bone (10–30 GPa) [1], and high mechanical strength [2], are being developed with non-toxic alloying elements such as niobium (Nb) and zirconium (Zr) to replace the traditional alloy Ti–6Al–4V. Niobium is added as it is a β-phase stabilizer and highly biocompatible [3] whereas Zr is a neutral element in terms of phase stabilization, even though some research work suggests that zirconium stabilizes the β-phase in the Ti–Nb–Zr system [4]. In addition, it is desirable to have the elastic modulus of the titanium alloy close to that of human bone. In implants, high Young's modulus results in bone resorption (stress shielding), while a low elastic modulus causes overloading [5].

Powder metallurgy (PM) has been successfully used in the production of several titanium alloys [6]. This method is excellent for near net-shape production of surgical implants due to some inherent advantages. These include capability of precisely adjusting the chemical composition, feasibility, reduced cost and reduction of modulus by introducing pores [1]. The powders used in PM can be prepared by the hydrogenation – dehydrogenation (HDH) process using metal scrap. This process introduces hydrogen atoms in the metal's interstitial sites to promote embrittlement of the metal. The hydrogenated metal is then mechanically ground to obtain a fine powder that is heated under vacuum to remove the hydrogen [7,8]. The advantages of HDH process for powder production are: It's low cost, better green density and improved in densification during sintering, control of oxygen content in sintered samples and the hydrogen emitted from the hydrogenated powders might become a protective atmosphere during powder sintering [7,9].

The composition of the titanium alloy was chosen using the orbital molecular method in which two parameters (B_0 and M_d) are determined theoretically. B_0 is the bond order, a measure of the covalent bond strength between Ti and an alloying element. M_d is the metal's d-orbital energy level which correlates with electronegativity and the radius of the metallic element [10]. It has been reported the elastic moduli values of titanium alloys decrease with increase in B_0 and M_d [10]. Thus, this method allows us to select alloys with elastic modulus close to human bone from the position of the alloy in the stability map, called the $B_0 - M_d$ map. As per this procedure, the alloy Ti–27Nb–13Zr with $B_0 = 2.867$ and $M_d = 2.480$ is located near in the $\alpha + \beta$ region with elastic modulus in the range of 60–70 GPa [10,11,12]. The advantage of $\alpha + \beta$ alloys is that they can be strengthened by heat treatment and have properties like high specific strength, fatigue resistance and excellent corrosion resistance [13,14]. Besides, these alloys are often used in several medical applications such as femoral hip stems, spinal components, fracture fixation plates, etc [14].

* Corresponding author.
E-mail address: mwdmendes@ipen.com (M.W.D. Mendes).

http://dx.doi.org/10.1016/j.msec.2016.03.052
0928-4931/

Titanium alloys are used as orthopedic and dental implants, but the bioactivity is not sufficient to attain adhesion between the implant and bone [15,16]. Therefore it is necessary to modify the metal surface to make it bioactive. There are several surface modification techniques and these include: mechanical methods (machining, grinding, polishing, blasting), chemical methods (acid-etching, hydrogen peroxide treatment, alkali-heating procedure, acid-alkali or acid-alkali pre-calcification procedure, surface-induced mineralization) and electrochemical methods (electro-crystallization, electrophoretic deposition, and anodic oxidation) [17,18].

After surface treatments using the methods mentioned above, the alloys can be made bioactive by forming a biomimetic coating on the surface [19]. The procedure to form a biomimetic coating has advantages over other methods of coating (plasma spray, sputter deposition and sol–gel). This procedure is a low temperature process and applicable to any heat sensitive substrate including polymers. It allows the formation of bioactive bone-like apatite crystals. It forms evenly and inside porous or complex implant geometries. It can also incorporate bone-growth-stimulating factors [20]. In addition, the biomimetic process helps form a biologically active apatite layer on the substrate after immersion in an artificially prepared supersaturated calcium and phosphate solution known as simulated body fluid (SBF) [21]. SBF is a solution that has inorganic ions in concentrations similar to that of human blood plasma but does not contain any cells or proteins [22].

The purpose of this research was to characterize the Ti–27Nb–13Zr alloy produced by PM, analyze the influence of milling time on the sintering process, determine the mechanical properties (elastic modulus and microhardness) and evaluate the biomimetic coating to verify if the alloy can be used in orthopedics or dental applications.

2. Materials and methods

The Ti–27Nb–13Zr alloy was prepared by mixing powders of TiH, NbH and ZrH. The NbH and ZrH powders were obtained by hydrogenating the respective metal scraps. TiH powder was purchased from Brats – Sintered Filters and specials metallic powders.

The hydrogenation temperature of zirconium and niobium were 650 and 700 °C, respectively, and this was done for 30 min. The heating rate to the hydrogenation temperature was 20 °C a minute and hydrogen gas pressure was 9.5 bar. A stainless steel recipient was used to crush the hydrogenated powders. The powders were then sieved (40 mesh) prior to milling. Before mixing the powders, pickling solutions were used to remove the impurities. A solution of distilled water and HNO_3 (10:1) was used for ZrH and a solution of H_2SO_4, HNO_3, HF and distilled water (5:2:2:1) was used for NbH. The powders to be characterized using various techniques were prepared by first weighing them in the right proportions followed by grinding in a Fritsh GmbH high-energy Pulverisette 7 Premium mill at a speed of 300 rpm and with a ball to powder ratio of 10:1 for 2, 6 and 10 h. The milling crucible was coated with zirconium oxide and the balls, 5 mm in diameter, were also made of the same material. The milling was carried out with cyclohexane (C_6H_{12}) after which the powders were dried by reducing the pressure in the milling chamber with a mechanical vacuum pump. The powder mixtures were characterized in terms of structure and composition by XRD analysis. The grain size distribution and morphology were studied using a SEM.

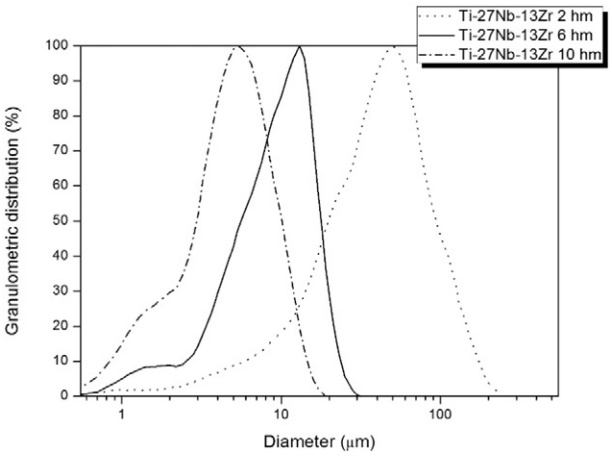

Fig. 2. Cumulative particle size distribution of Ti–27Nb–13Zr alloy powder.

The samples for SEM, XRD analysis, microhardness measurement and biomimetic coating, were uniaxially compacted in a 6.0 mm diameter matrix, with pressure of 65 MPa, followed by cold isostatic pressing (CIP) at 200 MPa during 60 s. The samples for measuring the Young's modulus were rectangular parallelepiped (40 × 6 × 2 mm) and these were compacted in a rectangular matrix at pressure of 6 MPa followed by CIP under conditions mentioned above. The lower pressure was used for shaping the specimen before CIP and sintering.

The sintering temperature in a high vacuum furnace was 1300 °C and the specimens were heated to this temperature at 5 °C/min until 500 °C, held for 1 h for dehydrogenation and then at 7 °C/min up to 1300 °C and held for 3 h. The sintered samples were mounted in epoxy resin and prepared for metallographic examination using conventional techniques. That is, the mounted specimens were ground using SiC sandpaper and then polished using colloidal silica (0.06 μm). The hardness measurements were performed in a Buehler Macrovickers 5112 equipment with a load of 300 g for 15 s. X-ray diffraction analysis was carried out in a Rigaku DMAX 2200 equipment, operating at 40 kV, 20 mA and copper radiation. The scanned range was 20° to 90° at a scan

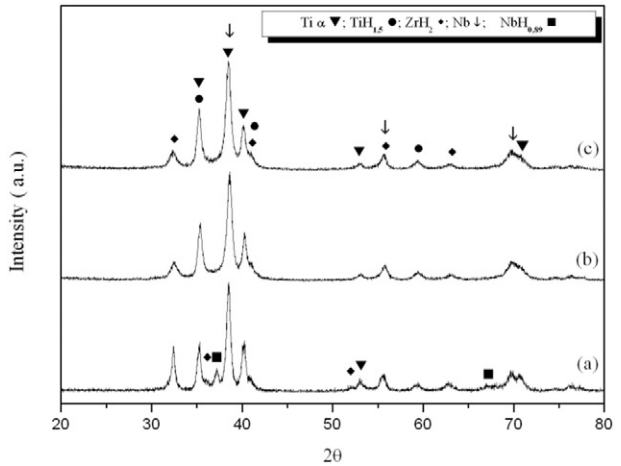

Fig. 1. XRD spectra of Ti–27Nb–13Zr after milling for (a) 2 h, (b) 6 h, and (c) 10 h.

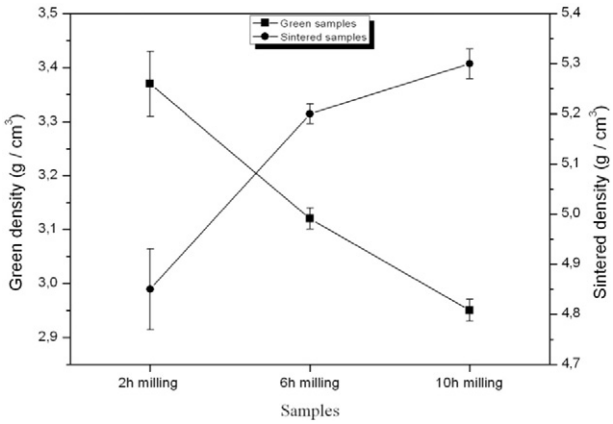

Fig. 3. Variation of density of samples prepared with powders milled for different times.

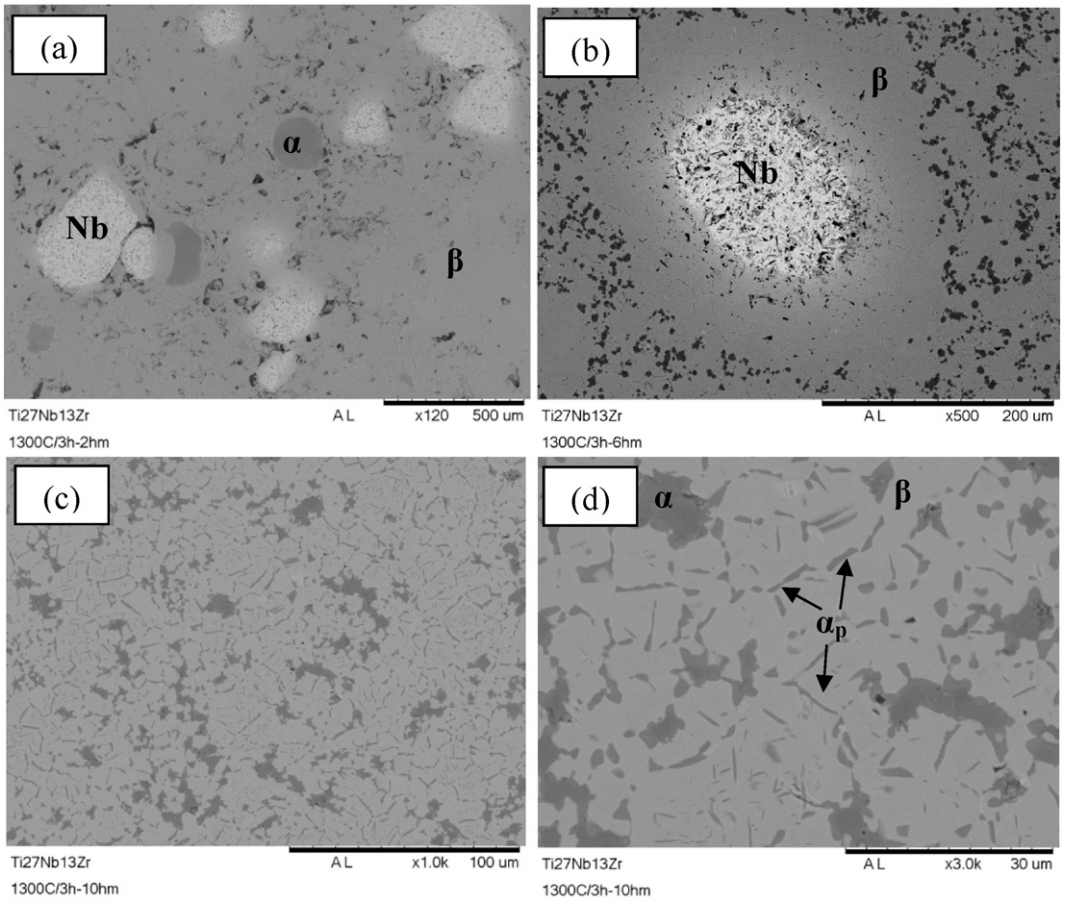

Fig. 4. Scanning electron micrographs of Ti–27Nb–13Zr milled for different duration and heat treated at 1300 °C for 3 h. (a) 2 h; (b) 6 h; (c) and (d) 10 h.

rate of 2°/min. The XRD patterns were compared with the PDF −2 database of the International Centre for Diffraction Data (ICDD). The elastic modulus of the alloy was determined by a dynamic method based on impulse excitation of vibration using a Grindosonic apparatus. The measurements were performed as per ASTM standards. Kroll solution was used for metallographic etching of samples, and the microstructure was observed in a Philips XL – 30 model scanning electron microscope (SEM).

To obtain the biomimetic coating, the sintered samples were first washed in an ultrasonic cleaner with acetone and ultrapure water (MilliQ, Millipore). After which they were given an alkali pre-treatment that consisted of soaking the samples in NaOH (5 M) solution at 60 °C for 24 h followed by washing with ultrapure water. The samples were then immersed in the SBF solution prepared by dissolution in ultrapure water of the following analytical grade reagents: NaCl, KCl, K_2HPO_4, $CaCl_2 \cdot 2H_2O$, $MgCl_2 \cdot 6H_2O$, $NaHCO_3$, and Na_2SO_4 [19]. The pH was adjusted with HCl 0.1 M and tris (hidroxymetilaminomethane) to 7.25 (36.5 °C). The samples were placed in separate polyethylene recipients containing SBF and held for 3, 7, 11 and 15 days under constant agitation. The SBF solution was renewed every three days. Finally, the samples were removed, washed in ultrapure water and dried at 40 °C.

The coated specimens were studied using diffuse reflectance FTIR spectroscopy (Thermo Nicolet 870 – NEXUS), scanning electron microscopy (SEM – Philips XL – 30) and XRD analysis.

Table 1
EDS analysis of α and β phases in microstructure of Fig. 4(d).

Phases	Ti (wt%)	Nb (wt%)	Zr (wt%)
α phase	78.0	10.0	12.0
β phase	59.5	28.5	12.0

3. Results and discussion

The hydrogenated powders that were used to prepare the Ti–27Nb–13Zr alloy revealed angular morphologies. Mean particle sizes of 130 and 170 μm for TiH and ZrH, respectively, while NbH < 425 μm.

The phases present in the powder mixtures after milling are hydrides ($TiH_{1,5}$, $NbH_{0,89}$ and ZrH_2), α-Ti and Nb as shown in Fig. 1. The ICDD codes used to identify the phases α-Ti, $TiH_{1,5}$, ZrH_2, Nb and $NbH_{0,89}$ were: 44–1294, 78–2216, 17–0314, 89–3715 and 7–0263 respectively. Peak broadening observed in Fig. 1 is due to structure

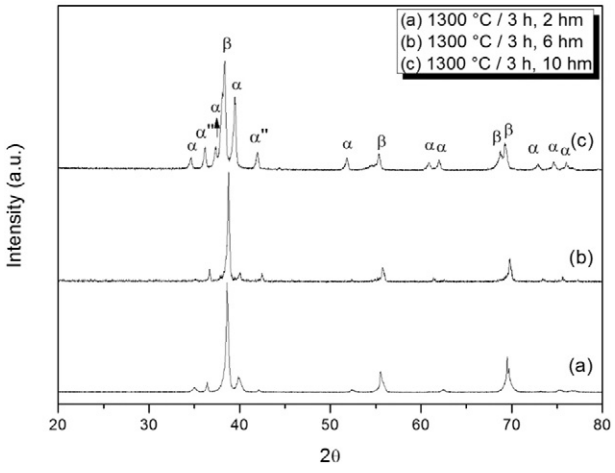

Fig. 5. XRD spectra of Ti–27Nb–13Zr alloy after sintering.

Table 2
Quantity of phases formed in Ti–27Nb–13Zr as determined by the Rietveld method.

TNZ	Ti-α (%)	Ti-β (%)	α″ phase(%)	σ
1300 °C/3 h–2 hm	14.47	83.27	2.37	2.70
1300 °C/3 h–6 hm	11.2	82.74	6.06	1.85
1300 °C/3 h–10 hm	30.11	53.55	16.34	2.01

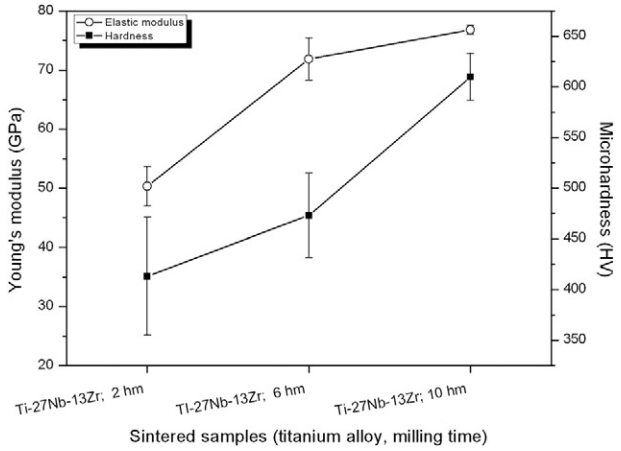

Fig. 6. Young's modulus and microhardness of specimens sintered at 1300 °C for 3 h.

distortion–introduction of atoms and/or defects. Displacement of the peaks is also associated with deformation of the crystal structure, due to dissolution of elements and the introduction of defects during the grinding process. The disappearance of the NbH peaks occurs due to formation of a solid solution in the crystal structure of titanium [23].

Fig. 2 shows the cumulative particle size distribution of Ti–27Nb–13Zr milled for 2, 6 and 10 h (hm – hours of milling).

The marked reduction in particle size with increase in milling time is due to increased number of collisions between the balls in the crucible and the alloy particles, promoting thereby the breaking-up of larger particles into smaller ones by the deformation and fracture process [23]. Smaller particle size contributes towards increased densification. In addition, the higher surface area of the smaller particles increases the number of bonds among the particles, and promotes more efficient solid state diffusion processes [24,25].

The green density and sintered density of the samples are shown in Fig. 3. As foreseen, there is a decrease in density due to reduction in particle size. In powders milled for 2 h (2 hm) the wider particle-size distribution, which includes large and small particles, favors stacking and higher green density as the smaller particles fit into the interstices between the large particles. Whereas in powders milled for 6 and 10 h the small particles provide a greater number of contacts, causing increased resistance to compaction. Thus the inter-particle friction increases with decreasing particle size, resulting in increased agglomeration and lower green density [26].

The calculated theoretical density of the alloy is 5.42 g cm^{-3}. The smaller particle size of powders milled for 6 and 10 h provides greater inter-particle contacts and therefore, more paths for process diffusion, thus increasing densification.

Fig. 4 shows scanning electron micrographs of Ti–27Nb–13Zr powders milled for 2, 4 and 6 h and heat treated at 1300 °C for 3 h. The sample in Fig. 4(a) shows several regions with undissolved niobium (white area), α-Ti (dark area) and the β-Ti matrix (light area). In Fig. 4(b), a micrograph of the sample with powder milled for 6 h, the Nb remained undissolved and more precipitates of α-Ti are visible. In Fig. 4(c) and (d), undissolved Nb is no longer seen and there are larger α-Ti colonies alongside α-plates (α_p). When titanium alloy is cooled

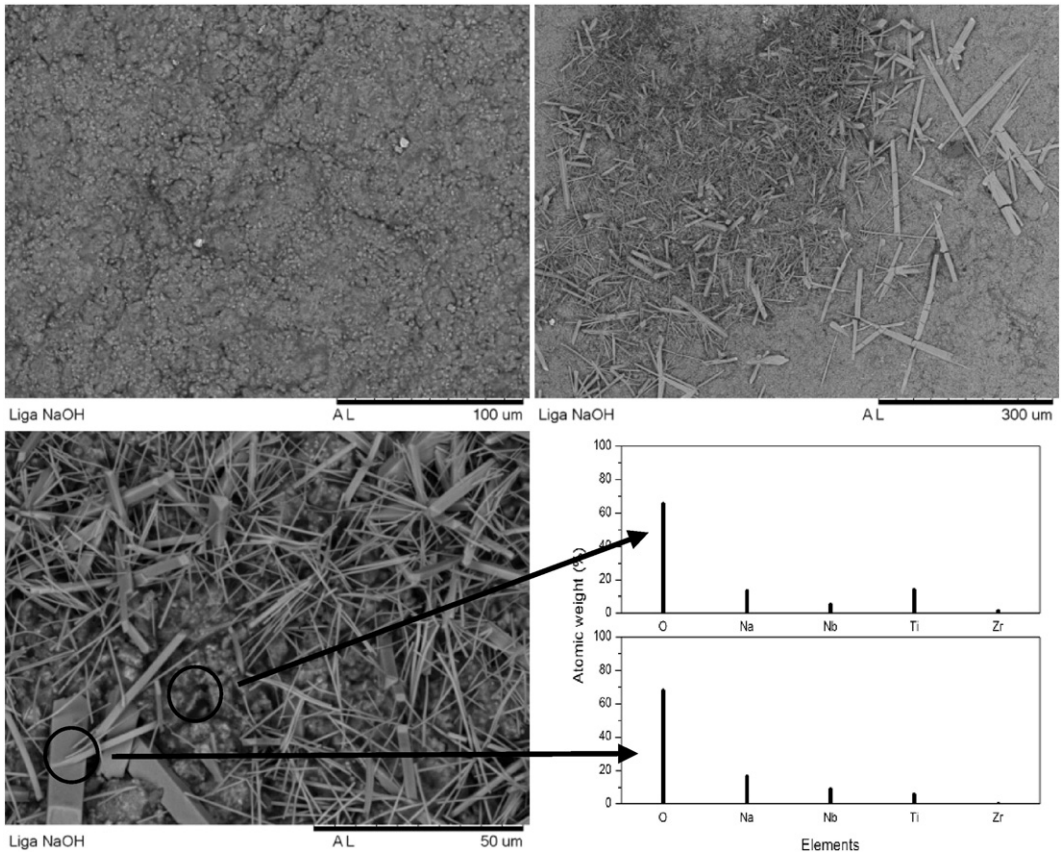

Fig. 7. Scanning electron micrographs of the surface of a sample treated with NaOH solution.

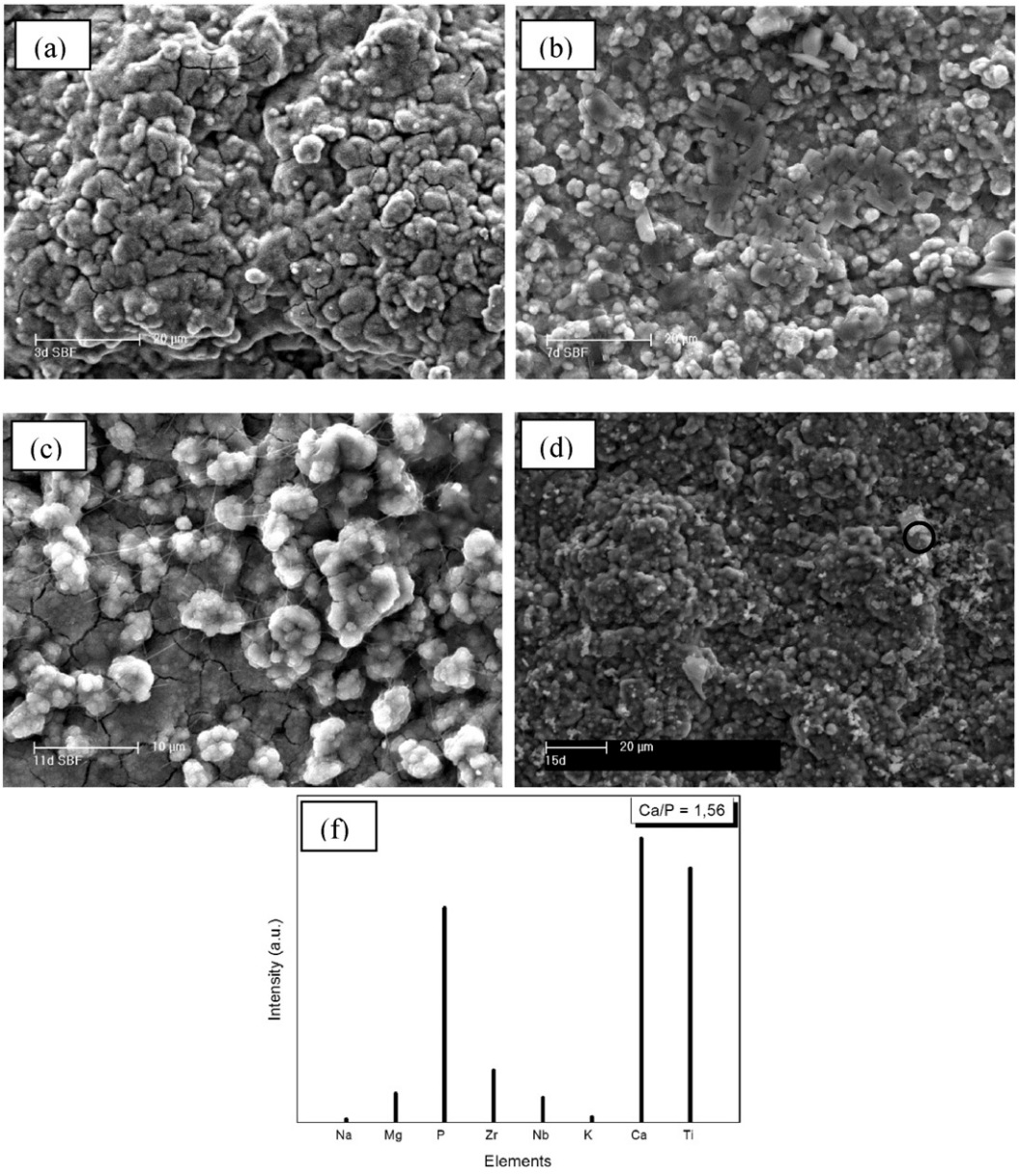

Fig. 8. SEM of samples after immersion in SBF for periods of: (a) 3 days; (b) 7 days; (c) 11 days; and (d) 15 days. The EDS of the region in the black circle in (d) is shown in (f).

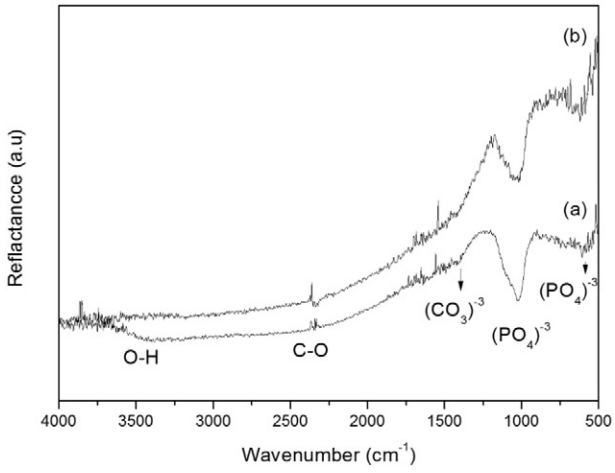

Fig. 9. Diffuse Reflectance Infrared Fourier Transform (DRIFT) analysis of samples immersed in SBF for periods of 3 (a) and 15 days (b).

from the β-phase regime, the α-phase nucleates from the β phase matrix [27]. In this investigation the samples were furnace cooled, which is a slow cooling process. Hence, the tendency to form α colonies in the β matrix.

EDS analysis at regions shown with black circles in Fig. 4d revealed the composition (semi-quantitative) shown in Table 1 of the α and β phases in samples prepared with powders milled for 10 h and sintered at 1300 °C for 3 h.

The alloy consists predominantly of the β-Ti phase (bcc) with some α-Ti (hcp) as shown in Fig. 5. The presence of the orthorhombic martensite α″ phase, caused by transition from the hexagonal α′ phase to the body centered cubic β phase, is due the amount of Nb (> 20%) in the alloy [28,29].

The quantity of phases formed in samples milled for different duration is given in Table 2. With increase in milling time, a decrease in quantity of the β phase occurs. It has been reported that in titanium alloy the α-phase exhibits higher elastic modulus compared with the β-phase. The elastic modulus of the different phases in titanium alloys increase in the sequence $\beta < \alpha'' < \alpha < \Omega$ [30].

The elastic modulus and microhardness of alloy samples prepared with powders milled for different duration and sintered at 1300 °C for 3 h are shown in Fig. 6. These mechanical properties increase with milling time of the powders and the quantity of α and β phases. Samples prepared with powders milled for 2 h had lower modulus values (50 GPa), akin to human bone, but the hardness was low that could lead to greater wear out. Nevertheless, these specimens still revealed undissolved niobium.

The samples with a higher amount of α phase (TNZ 1300 °C/3 h – 2 hm and TNZ 1300 °C/3 h – 10 hm) exhibited greater hardness than the specimens with a predominance of β phase. This is due to higher deformation resistance of hcp structures (α phase) compared to bcc structures (β phase) [2].

The samples prepared with powders milled for 10 h and sintered at 1300 °C for 3 h exhibited modulus values close to that of Ti–13Nb–13Zr alloy [28,29], and high hardness meeting the requirement for long service life (over 20 years) as bone implants in young patients [31].

Samples that were more homogeneous (1300 °C/3 h and 10 h milling) were used to form the biomimetic coatings. Fig. 7 shows scanning electron micrographs of samples treated with 5 M NaOH to form functional groups essential for adhesion of apatites that form when the substrate is immersed in SBF. Note the textured surface with irregular relief in Fig. 7(a) and regions with rods and/or needles in Fig. 7(b) and (c).

The EDS analysis showed the presence of the elements Nb, Ti and Zr, and a considerable quantity of O and Na, indicating formation of sodium titanate. The formation of titanate is due to partial dissolution of the passive TiO_2 layer in the NaOH solution, owing to the corrosive attack of OH^- ions producing titanate hydrogel layer on the surface of the substrates [32,33]. This product reacts with Na^+ present in the aqueous solution forming sodium titanate [34], which contributes to Ti–OH formation.

It has been reported in literature [34] that if there are enough Ti–OH groups on the surface, the calcium ions can accumulate on the surface so that the surface can gain an overall positive charge. Thus, negatively charged phosphate ions to form amorphous calcium phosphate that spontaneously transforms into the apatite, because, the apatite is the stable phase in body environment.

The surfaces of specimens immersed in SBF for 3, 7, 11 and 15 days are shown in Fig. 8. Formation of a layer of globular apatite on the surface can be seen. The cracks seen in Fig. 8(c) formed during the drying process. Upon exposure to the SBF, the samples release the Na^+ ion from the sodium titanate layer into the SBF via exchange with H_3O^+ ions in the fluid, increasing thus the OH^- concentration and the ionic activity of the surrounding fluid, to form Ti–OH groups on the surface of the titanium coating. These groups are negatively charged and combine with the positively charged Ca_2^+ ions in the fluid to form calcium titanate. This combination creates an overall positive charge on the surface. Subsequently, the calcium titanate (positively charged) combines with the phosphate ions (negatively charged) to form amorphous calcium phosphate, which transforms into apatite [34,15,35].

The DRIFT analysis spectrums shown in Fig. 9, reveal the presence of well-defined bands of O–H at 3500 cm^{-1}, $(PO_4)^{-3}$ at 1010 and 600 cm^{-1}, and $(CO_3)^{-2}$ at 1400 and 1500 cm^{-1} in samples immersed in SBF for 3 and 15 days. The specimens immersed for 7 and 11 days also show the same bands. Thus the presence of these bands in all of the samples together with the EDS analysis results shown in Fig. 7(f) suggests the formation of apatite [10].

4. Conclusions

The alloy is classified as α + β, and the milling time influences the formation of these phases. In this case, increase in milling time revealed a tendency for α″ phase to increase. In the alloys prepared with powders milled for 2 and 6 h there is a greater quantity of β-Ti phase than α-Ti.

Increase in milling time to 10 h resulted in an equiaxed structure with α-plates and α-colonies in the β matrix, with all the niobium in solution. The microstructure and dissolution of Nb are directly related to the mechanical properties of the alloy, that is, increase in microhardness and Young's modulus.

Evaluation of the biomimetic coating showed that it is possible to form apatite on all samples immersed in SBF for 3 or more days.

The results obtained from evaluation of specimens immersed in SBF and the mechanical properties indicate that the alloy prepared with milling time to 10 h can be used in orthopedic applications (femoral stem or femoral head) or in dental applications.

Acknowledgements

The authors acknowledge the financial support of Capes (scholarship granted to M.W.D. Mendes and C. G. Ágreda), CNPq (grant n° 307954/2013-7) and FAPESP (grant n° 2008/57860-3).

References

[1] F.A. Müller, M.C. Bottino, L. Müller, V.A.R. Henriques, U. Lohbauers, A.H.A. Bressiani, J.C. Bressiani, In vitro apatite formation on chemically treated (P/M) Ti–13Nb13Zr, Dent. Mater. 24 (2008) 50–56, http://dx.doi.org/10.1016/j.dental.2007.02.005.
[2] A. Nouri, X. Chen, Y. Li, Y. Yamada, P.D. Hodgson, C. Wen, Synthesis of Ti–Sn–Nb alloy by powder metallurgy, Mater. Sci. Eng. A 485 (2008) 562–570, http://dx.doi.org/10.1016/j.msea.2007.10.010.
[3] D. Zhao, K. Chang, T. Ebel, M. Quian, R. Willumeit, M. Yan, F. Pyczak, Microstructure and mechanical behavior of metal injection molded Ti–Nb binary alloy as biomedical material, J. Mech. Behav. Biomed. Mater. 29 (2013) 171–182, http://dx.doi.org/10.1016/j.jmbbm.2013.08.013.
[4] W. Simka, A. Krzala, M. Maselbas, G. Dercz, J. Szade, A. Winiarski, J. Michalska, Formation of bioactive coatings on Ti–13Nb–13Zr alloy for hard tissue implants, RSC Adv. 3 (2013) 11195–11204, http://dx.doi.org/10.1039/c3ra23256e.
[5] G. He, M. Hagiwara, Bimodal structured Ti-base alloy with large elasticity and low Young's modulus, Mater. Sci. Eng. C 25 (2005) 290–295, http://dx.doi.org/10.1016/j.msec.2005.03.001.
[6] M.C. Bottino, P.G. Coelho, V.A.R. Henriques, O.Z. Higa, A.H.A. Bressiani, J.C. Bressiani, Processing, characterization, and in vitro/in vivo evaluations of powder metallurgy processed Ti–13Nb–13Zr alloys, J. Biomed. Mater. Res. A 88 (2009) 689–696, http://dx.doi.org/10.1002/jbm.a.31912.
[7] S.B. Gabriel, G. Silva, K.C.G. Candioto, I.D. Santos, P.A. Suzuki, C.A. Nunes, Niobium hydrogenation process: effect of temperature and cooling rate from the hydrogenation temperature, Int. J. Refract. Met. Hard Mater. 29 (2011) 134–137, http://dx.doi.org/10.1016/j.ijrmhm.2010.09.006.
[8] K.C.G. Candioto, C.A. Nunes, Nb–20%Ta alloy powder by the hydriding–dehydriding technique, Int. J. Refract. Met. Hard Mater. 24 (2006) 413–417, http://dx.doi.org/10.1016/j.ijrmhm.2005.06.001.
[9] X. Rao, C.L. Chun, Y.Y. Zheng, Phase composition, microstructure and mechanical properties of porous Ti–Nb–Zr alloys prepared by a two step foaming powder metallurgy method, Int. J. Refract. Met. Hard Mater. 29 (2011) 27–36, http://dx.doi.org/10.1016/j.jmbbm.2014.02.001.
[10] D. Kuroda, M. Niinomi, M. Morinaga, Y. Kato, T. Yashiro, Design and mechanical properties of new β type titanium alloys for implant materials, Mater. Sci. Eng. A 243 (1998) 244–249, http://dx.doi.org/10.1016/S0921-5093(97)00808–3.
[11] H.P. Ng, E. Douguet, C.J. Bettles, B.C. Muddle, Age-hardening behavior of two metastable beta-titanium alloys, Mater. Sci. Eng. A 527 (2010) 7017–7026, http://dx.doi.org/10.1016/j.msea.2010.07.055.
[12] M. Abdel-Hady, K. Hinoshita, M. Morinaga, General approach to phase stability and elastic properties of β-type Ti-alloys using electronic parameters, Scr. Mater. 55 (2006) 477–480, http://dx.doi.org/10.1016/j.scriptamat.2006.04.022.
[13] R. Chen, G.A. Thous, Metallic implant materials, Mater. Sci. Eng. R 87 (2015) 1–57, http://dx.doi.org/10.1016/j.mser.2014.10.001.
[14] P. Barriobero-Vila, G. Requena, T. Buslaps, M. Alfeld, U. BoesenBerg, Role of element partitioning on the α-β phase transformation kinetics of a bi-modal Ti–6Al–6V–2Sn alloy during continuos heating, J. Alloys Compd. 626 (2015) 330–339, http://dx.doi.org/10.1016/j.jallcom.2014.11.176.
[15] T. Kokubo, H.-M. Kim, M. Kawashita, Novel bioactive materials with different mechanical properties, Biomaterials 24 (2003) 2161–2175, http://dx.doi.org/10.1016/S0142-9612(03)00044–9.
[16] E.C.S. Rigo, A.O. Boschi, M. Yoshimoto, S. Allegrini Jr., B. Konig Jr., M.J. Carbonari, Evaluation in vitro and in vivo of biomimetic hydroxyapatite coated on titanium dental implants, Mater. Sci. Eng. C 24 (2004) 647–651, http://dx.doi.org/10.1016/j.msec.2004.08.044.
[17] B. Feng, J.Y. Chen, S.K. Qi, L. He, J.Z. Zhao, X.D. Zhang, Carbonate apatite coating on titanium induced rapidly by precalcification, Biomaterials 23 (2002) 173–179, http://dx.doi.org/10.1016/S0142-9612(01)00093-X.
[18] S. Izman, et al., Surface modification techniques for biomedical grade of titanium alloys: oxidation, carburization and ion implantation processes, Titanium Alloys — Towards Achieving Enhanced Properties for Diversified Applications 2012, pp. 201–228, http://dx.doi.org/10.5772/36318.
[19] C.G. Ágreda, M.W.D. Mendes, J.C. Bressiani, A.H.A. Bressiani, Apatite coating on titanium samples obtained by powder metallurgy, Adv. Sci Technol. 86 (2013) 28–33, http://dx.doi.org/10.4028/www.scientific.net/AST.86.28.

[20] W.S. Medeiros, M.V. Oliveira, L.C. Pereira, M.C. Andrade, Bioactive porous titanium: Na alternative to surgical implants, Artif. Organs 32 (2008) 277–282, http://dx.doi.org/10.1111/j.1525-1594.2008.00543.x.
[21] T. Kokubo, H. Takadama, How useful is SBF in predicting in vivo bone bioactivity? Biomaterials 27 (2006) 2907–2915, http://dx.doi.org/10.1016/j.biomaterials.2006.01.017.
[22] M. Kamitakahara, C. Ohtsuki, T. Miyazaki, Coating of bone-like apatite for development of bioactive materials for bone reconstruction, Biomed. Mater. 2 (2007) 17–23, http://dx.doi.org/10.1088/1748-6041/2/4/R01.
[23] C. Suryanarayana, Mechanical alloying and milling, Prog. Mater. Sci. 46 (2001) 1–184, http://dx.doi.org/10.1016/S0079-6425(99)00010–9.
[24] G.S. Upadhyaya, Powder Metallurgy Technology, first ed. Cambridge International Science Publishing, 2002.
[25] J.S. Hirschhorn, Introduction to Powder Metallurgy, 2th ed. American Powder Metallurgy Institute, Princeton, New Jersey, 1976.
[26] A. Nouri, P.D. Hodgson, C.E. Wen, Effect of process control agent on the porous structure and mechanical properties of a biomedical Ti–Sn–Nb alloy produced by powder metallurgy, Acta Biomater. 6 (2010) 1630–1639, http://dx.doi.org/10.1016/j.actbio.2009.10.005.
[27] G. Lütjering, J.C. Wiliams, Titanium, 2th ed. Springer, Berlin, 2007.
[28] C.R.M. Afonso, G.T. Aleixo, A.J. Ramirez, R. Caram, Influence of cooling rate on microstructure of Ti–Nb alloy for orthopedic implants, Mater. Sci. Eng. C 2 (2007) 908–913, http://dx.doi.org/10.1016/j.msec.2006.11.001.
[29] T. Ahmed, H.J. Rack, Martensitic transformation in Ti–(16–26 at%)Nb alloys, J. Mater. Sci. 31 (1996) 4267–4276, http://dx.doi.org/10.1007/BF00356449.
[30] P. Majumdar, S.B. Singh, M. Chakraborty, Elastic modulus of biomedical titanium alloys by nano-indentation and ultrasonic techniques—a comparative study, Mater. Sci. Eng. A 489 (2008) 419–425, http://dx.doi.org/10.1016/j.msea.2007.12.029.
[31] S.B. Gabriel, J. Dille, C.A. Nunes, G.A. Soares, The effect of niobium content on the hardness and elastic modulus of heat-treated Ti–10Mo–Xnb Alloys, Mater. Res. 13 (2010) 333–337, http://dx.doi.org/10.1590/S1516-14392010000300009.
[32] C.M. Assis, L.C.O. Vercik, M.L. Santos, M.V.L. Fook, A.C. Guastaldi, Comparision of cristallinity between natural hydroxyapatite and synthetic cp-Ti/HA coatings, Mater. Res. 8 (2005) 207–211, http://dx.doi.org/10.1590/S1516-14392005000200022.
[33] K. Lee, D. Yoo, Large-area sodium titanate nanorods formed on titanium surface via NaOH alkali treatment, Arch. Metall. Mater. 60 (2015) 1371–1374, http://dx.doi.org/10.1515/amm-2015-0133.
[34] Y. Chen, X. Zheng, H. Ji, C. Ding, Effect of Ti–OH formation on bioactivity of vacuum plasma sprayed titanium coating after chemical treatment, Surf. Coat. Technol. 202 (2007) 494–498, http://dx.doi.org/10.1016/j.surfcoat.2007.06.015.
[35] H.M. Kim, F. Miyaji, T. Kokubo, T. Nakamura, Effect of heat treatment on apatite-forming ability of Ti metal induced by alkali treatment, J. Mater. Sci. Mater. Med. 8 (1997) 341–347, http://dx.doi.org/10.1023/A:1018524731409.